# STAU - A GENERAL-PURPOSE TOOL FOR PROBABILISTIC RELIABILITY ASSESSMENT OF CERAMIC COMPONENTS UNDER MULTIAXIAL LOADING

H. Riesch-Oppermann [1], A. Brückner-Foit [2] and C. Ziegler[2]

[1] Forschungszentrum Karlsruhe, Institut für Materialforschung II,
P.O. Box 3640, D-76021 Karlsruhe, FRG
[2] Universität Karlsruhe, Institut für Zuverlässigkeit und Schadenskunde im Maschinenbau,
P.O. Box 3640, D-76021 Karlsruhe, FRG

## ABSTRACT

Lack of appropriate design tools is one of the facts that hinders ceramics from being widely applied as structural material with high strength, good resistance against wear and corrosion, strong high temperature durability and favourable thermal properties. Ceramics design methods differ completely from design methods for metals as they are based on fracture statistics rather than on maximum tolerable stresses. During the past few years, the post-processing tool STAU (STatistical Analysis of ceramic components Under various loading conditions) has been developed. As a back-end to the general-purpose Finite Element code ABAQUS, STAU is able to generate failure probabilities from stress analysis results. Additionally, a local risk of fracture is calculated. From this it is possible to identify critical regions and to modify the component design accordingly. In its basic form, STAU deals with fracture due to unstable crack extension under static loading. Several additional modules are available to deal with more general situations, e.g. STAULE for subcritical crack growth and time-dependent loading and STAUB for the analysis of proof tests. The capabilities of the code are illustrated by several examples taken from applications of ceramics materials in gas turbines operating at very high temperatures.

## INTRODUCTION

The failure behaviour of monolithic ceramic materials can be well described by the multiaxial Weibull theory [1-4] and its extensions [5,6]. The lifetime distribution can be predicted for components on the basis of test results obtained with laboratory specimens of very simple shape such as four-point bend bars. In this sense, ceramics are very well understood. Design of ceramics is always reliability based due to the inherent scatter of the fracture strength caused by the presence of natural flaws. Codes are currently available which allow a probabilistic design under constant [7] or general time-dependent loading [8]. Temperature-dependent material properties can also be taken into account [8,12].

## REVIEW OF MULTIAXIAL WEIBULL THEORY

In the multiaxial Weibull theory it is assumed that failure of ceramic materials is caused by the unstable extension of natural flaws of random size, random location, and random orientation with respect to the principal stress axes. The worst flaw, i.e. the flaw with the worst combination of size, orientation, and stress determines the maximum tolerable load.

***Spontaneous failure***

The probability that the size $a$ of a given flaw exceeds its critical size $a_c$ is given by

$$Q_1 = \frac{1}{2\pi A} \cdot \int_0^{2\pi} \int_A (1 - F_a(a_c))\, \mathrm{d}A\mathrm{d}\phi \tag{1}$$

where $A$ denotes the surface area of the component considered, $\phi$ is the orientation of the flaw and $F_a(\cdot)$ is the probability distribution function of the flaw size. A fracture mechanics model is used to define the critical crack size $a_c$. Failure occurs, if the equivalent mode $I$ stress intensity factor, $K_{Ieq}$, exceeds the fracture toughness $K_{Ic}$, where $K_{Ieq}$ depends on the mode $I$-$III$ stress intensity factors of the crack and hence on the geometry of the crack and on the multiaxial stress field. An equivalent stress can be introduced by:

$$K_{Ieq} = \sigma_{eq} \sqrt{a} Y_I \tag{2}$$

where $Y_I$ is the fracture mechanics mode $I$ correction factor. The critical crack size is defined by solving Eqn.2 at $K_{Ic} = K_{Ieq}$.

Eqn. 1 is the failure probability for a component containing exactly one flaw. A component containing exactly $k$ non-interacting flaws fails, if at least one flaw starts to extend unstably, i.e.

$$Q_k = 1 - (1 - Q_1)^k \tag{3}$$

The actual number of flaws in a specific component is a random quantity which follows a Poisson distribution with the probability $p_k$ of having exactly $n$ flaws given by:

$$p_k = \frac{M^k}{k!} \cdot e^{-M} \tag{4}$$

where $M$ is the average number of flaws in the component. The probability $P_f$ of finding a component which contains exactly $k$ flaws and fails is just the product $1 - p_k \cdot (1 - Q_k)$. Summing over all possible values of $k$ finally leads to the following expression for the failure probability

$$\begin{aligned} P_f &= 1 - \sum_{k=0}^{\infty} \frac{M^k}{k!} \cdot e^{-M} \cdot (1 - Q_1)^k \\ &= 1 - \exp(-M \cdot Q_1) \end{aligned} \tag{5}$$

where the normalization condition of the Poisson distribution has been taken into account. Inserting eqs.(1),(2) into eq.(5) and using the asymptotic form of the flaw size distribution given by the statistical extreme value theory finally leads to the final expression for the failure probability:

$$P_f = 1 - \exp\left( - \frac{1}{2\pi A_0} \int_0^{2\pi} \int_A \left( \frac{\sigma_{eq}}{\sigma_0} \right)^m \mathrm{d}A\mathrm{d}\phi \right) \tag{6}$$

with the Weibull parameters $m$ and $\sigma_0$ characterizing the flaw distribution and the normalization area $A_0$. A similar relation can be obtained for volume flaws.

***Time-dependant failure***

Under sustained loading, subcritical crack growth may lead to a time-dependant flaw population and thus to an increase of the failure probability in time. Crack growth is governed by the stress intensity factor $K$ and the crack growth rate $v$ and is generally described by a power-law relation

$$v = AK_I^n \text{ or } v = A^*\left(\frac{K_I}{K_{Ic}}\right)^n \tag{7}$$

with parameters *A*, *A** and *n* depending on material, temperature, and environment [9]. For a constant geometry function $Y_I$ (see Eqn. 2) it is possible to obtain a closed-form solution for the crack size *a(t)* at time *t* by integrating the crack growth law (7). For $n \neq 2$, *a(t)* is given by

$$a(t) = \left( a_i^{\frac{2-n}{n}} + \frac{(2-n)AY_I^{\,n}}{2} \int_0^t (\sigma_{eq}(\tau))^n \,\mathrm{d}\tau \right)^{\frac{2}{2-n}} \tag{8}$$

Failure occurs at time *t*, if *a(t)* exceeds the critical crack size $a_c$ given by Eqn. 2 for $K_{Ieq} = K_{Ic}$. The critical crack size $a_c$ is time-dependant for time-dependent stress fields, and failure occurs for $a \geq a_c(\tau)$ at any instant $0 \leq \tau \leq t$. The failure condition can be re-written in terms of the initial flaw sizes occurring in Eqn. 8 leading to $a_i \geq \min_{\tau \in (0,t)}(a_{c,i}(\tau))$, where $a_{c,i}(\tau)$ is the initial flaw size corresponding to $a_c(\tau)$. Using the same line of arguments as for the deviation of Eqn 6, the following relation is obtained for the lifetime distribution [5]. The time-dependant failure probability is

$$P_f(t) = 1 - \exp\left\{ -\frac{1}{2\pi A_0} \int_0^{2\pi} \int_A \max_{\tau \in (0,t)} \left\{ \left[ \left( \frac{\sigma_{eq}(\tau)}{\sigma_0} \right)^{n-2} + \frac{\sigma_0^2}{B} \int_0^{\tau} \left( \frac{\sigma_{eq}(t')}{\sigma_0} \right)^n \mathrm{d}t' \right]^{\frac{1}{n-2}} \right\}^m \mathrm{d}A\mathrm{d}\phi \right\} \tag{9}$$

with $B = \frac{2}{(n-2)AY^2} K_{Ic}^{2-n}$. Eqn (9) is derived for the case that inert strength and lifetime are governed by the same flaw population. This assumption is violated if e.g. volume flaws with moderate sub-critical growth are relevant for the strength at $t = 0$, whereas the lifetime at $t \geq 0$ is determined by surface flaws which tend to grow rapidly in an aggressive environment. For strong stress gradients due to the presence of e.g. thermal shock loading, variation of the stress field along the crack has to be taken into account [10].

It can be shown [5] that for cyclic loading the lifetime follows a Weibull distribution if Eqn (7) governs crack extension, i.e. if effects of cyclic fatigue crack growth can be neglected. The distribution of the time to failure after *N* cycles of length *T* due to sub-critical crack growth and in case of large *N* is

$$P_f(N \cdot T) = 1 - \exp\left\{ -\frac{1}{2\pi A_0} \int_A \int_0^{2\pi} \left[ \frac{\sigma_0^2}{B} \cdot N \cdot \int_0^T \left( \frac{\sigma_{eq}(t')}{\sigma_0} \right)^n \mathrm{d}t' \right]^{\frac{m}{n-2}} \mathrm{d}\phi\mathrm{d}A \right\} \tag{10}$$

where the contribution of the inert strength was neglected compared to the time integral (which is appropriate for large values of *N*) and the periodicity of the loading cycles was taken into account. Thus for long times $t = N \cdot T$, the probability of failure after *N* cycles is $P_f(N) = 1 - \exp(-D \cdot N^{m^*})$ which is a Weibull distribution with the Weibull modulus

$$m^* = m/(n-2)$$

and with

$$D = \frac{1}{2\pi A_0} \int_A \int_0^{2\pi} \left[ \frac{\sigma_0^2}{B} \cdot \int_0^T \left( \frac{\sigma_{eq}(t')}{\sigma_0} \right)^n \mathrm{d}t' \right]^{\frac{m}{n-2}} \mathrm{d}\phi\mathrm{d}A .$$

Complex loading histories of components may thus be simulated by using suitable combinations of cyclic and constant loading intervals.

## IMPACT OF PROOF TEST ON COMPONENT RELIABILITY

The reliability of components that enter into service may be considerably improved by a preceding proof test at an appropriately chosen load level. Neglecting sub-critical crack growth during proof test time, $t_p$, the probability of failure of a component that did not fail during the proof test is given by [5]

$$P_f = 1 - \exp\left\{ -\frac{1}{2\pi A_0} \int_0^{2\pi} \int_A \left( \left( \frac{\sigma_{eq}^{(s)}}{\sigma_0} \right)^m - \left( \frac{\sigma_{eq}^{(p)}}{\sigma_0} \right)^m \right) \cdot \Theta\left( \sigma_{eq}^{(s)} - \sigma_{eq}^{(p)} \right) \mathrm{d}A \mathrm{d}\phi \right\} \tag{11}$$

for surface flaws with $\sigma_{eq}^{(p)}$ and $\sigma_{eq}^{(s)}$ denoting the proof test and service loads, respectively and $\Theta(\cdot)$ the Heaviside step function. Sub-critical crack growth during and after proof test can be considered as well in the context of time dependent loading. The result is a generalization of Eqn. (9) with additional contributions from proof test loading similar to those in Eqn. (11). The final expression is quite complicated but the numerical evaluation is straightforward. Details are given in [5].

## THE LOCAL RISK OF FRACTURE

Critical regions in a component have to be identified on the basis of fracture statistical reasoning. Let $A_t$ be a subsurface area of the component, the local risk of fracture is defined as the conditional probability that fracture starts in $A_t$ provided that failure occurred. Taking $A_t$ infinitesimally small, we obtain the density of the local risk of fracture $\pi(\underline{x})$ as

$$\pi(\underline{x}) = \frac{\frac{1}{2\pi} \int_0^{2\pi} \left( \frac{\sigma_{eq}}{\sigma_0} \right)^m \mathrm{d}\phi}{\frac{1}{2\pi} \int_0^{2\pi} \int_A \left( \frac{\sigma_{eq}}{\sigma_0} \right)^m \mathrm{d}A \mathrm{d}\phi} \tag{12}$$

which is a regular probability density function and obeys the normalization condition $\int_A \pi(\underline{x}) \mathrm{d}A = 1$ .The local risk of fracture $\pi(\underline{x})$ as given in Eqn. 12 allows to identify critical regions in a component and is a valuable tool for design improvements. Visualization of $\pi(\underline{x})$ is possible with commonly used graphical FE postprocessors. Formulation of Eqn. 12 for volume flaws is obvious.

## EXAMPLE: FAILURE BEHAVIOUR OF A CERAMIC BOLT IN A HIGH TEMPERATURE APPLICATION

A ceramic bolt as part of an experimental combustion chamber was used in Ref. [12] as model component for the demonstration of the STAU capabilities. A pressure-less sintered silicon carbide (SSiC) was used as material. The Weibull modulus of the material from four point bend tests was $m = 9.5$. Assuming that failure of natural flaws is determined by mode-I loading, a 'true' Weibull parameter of $\sigma_{0,V} = 358$ MPa was obtained from the four point bend results where failure is assumed to be caused by volume flaws. For sub-critical crack growth, a crack growth exponent of $n$=20 was used.

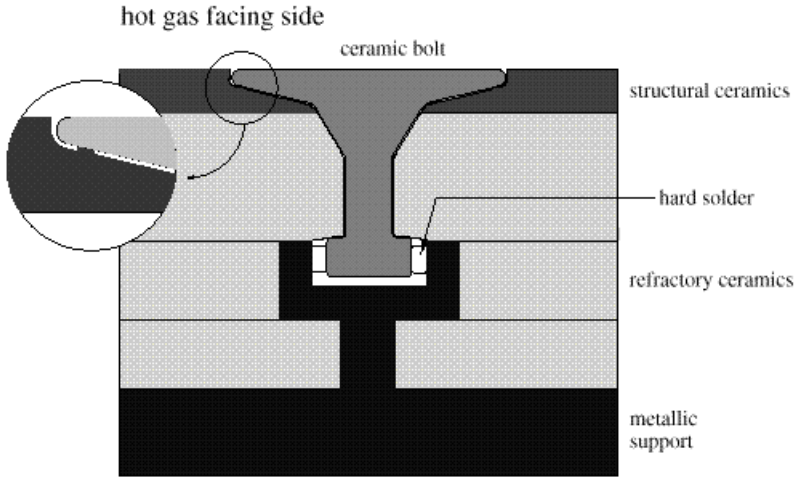


**Figure 1:** Ceramic fastener bolt in the thermal barrier lining of a combustion chamber.

The bolt geometry is shown in Fig. 1. A combined thermal and mechanical loading situation is present which is indicated in the left and right part of the Finite Element mesh shown in Figure 2 (only half of the structure is shown because of symmetry). The mechanical loading is due to the fixture of the bolt, whereas the thermal loading is generated by the temperature difference between parts of the bolts facing hot gas and cooling air, respectively.

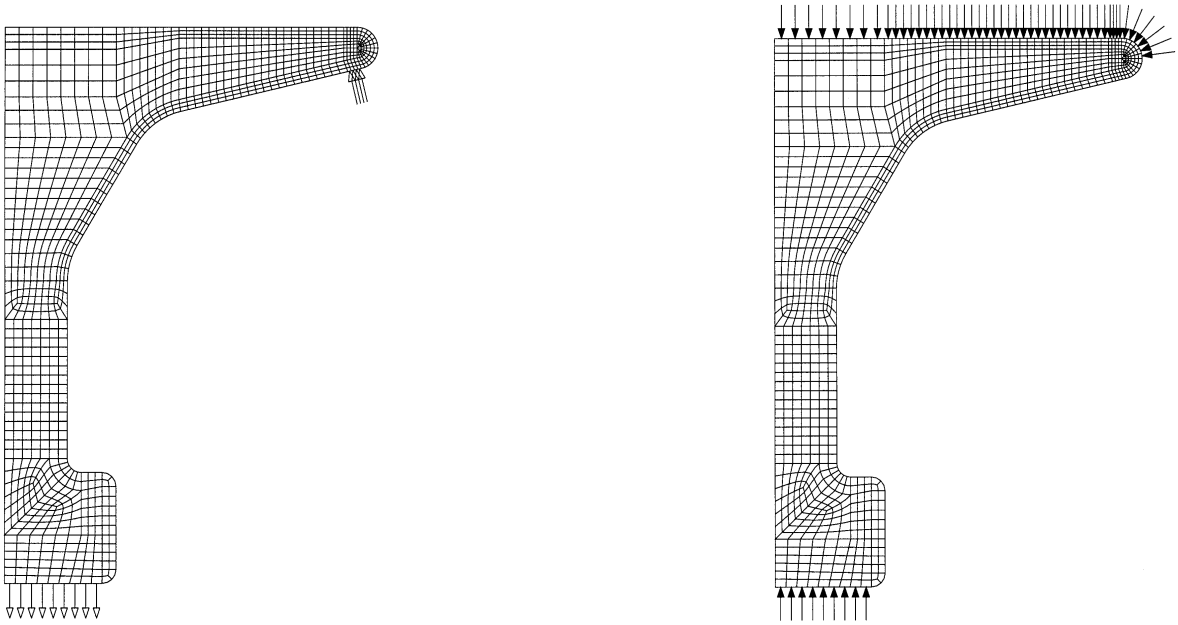

**Figure 2:** FE mesh with mechanical (left) and thermal (right) loading conditions of the bolt.

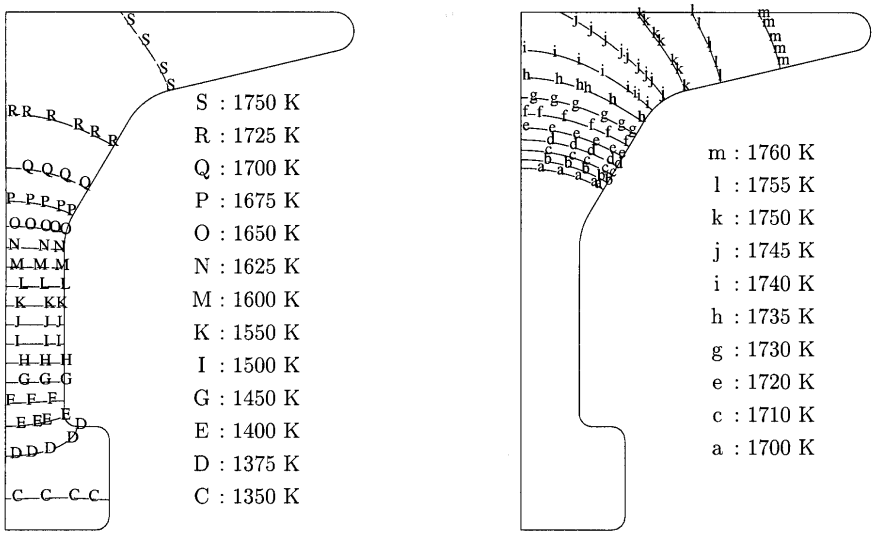


**Figure 3:** Temperature distribution under stationary loading conditions.

For stationary loading conditions, the temperature distribution is shown in Fig. 3. A maximum temperature of about $T$=1760 K is present for the chosen thermal boundary conditions for temperatures of hot gas and cooling air and the given coefficients of thermal conductivity. The corresponding results for the maximum principal stress are shown in Fig. 4. The maximum value of the stress distribution is at the centre of the bolt surface facing the hot gas side. The failure probability and the local risk of fracture can be obtained using STAU from the stress distribution. The results are given in Fig. 5. As expected from the stress distribution, the local risk of fracture has its maximum near the centre of the bolt surface; however, as shown in the inset of Fig. 5, the maximum of the local risk of fracture is shifted from the centre to a location to a point about 3 mm off the axis. This is due to size effect and reflects the influence of the stressed volume which increases proportionally to the distance from the axis due to the axial symmetry of the bolt geometry.

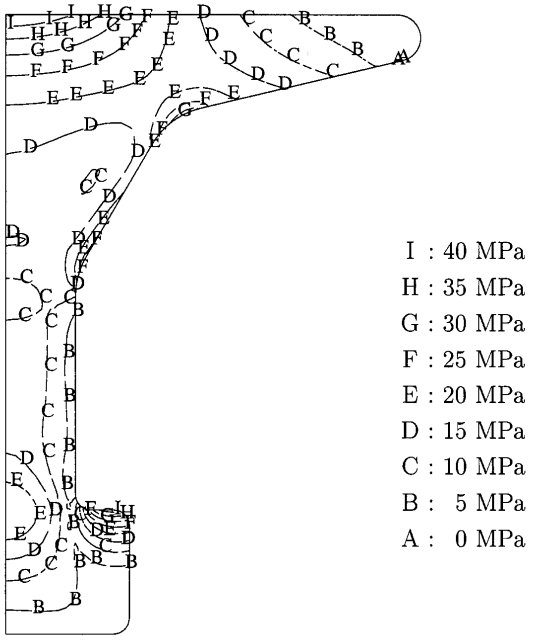


**Figure 4:** Maximum principal stress contours.

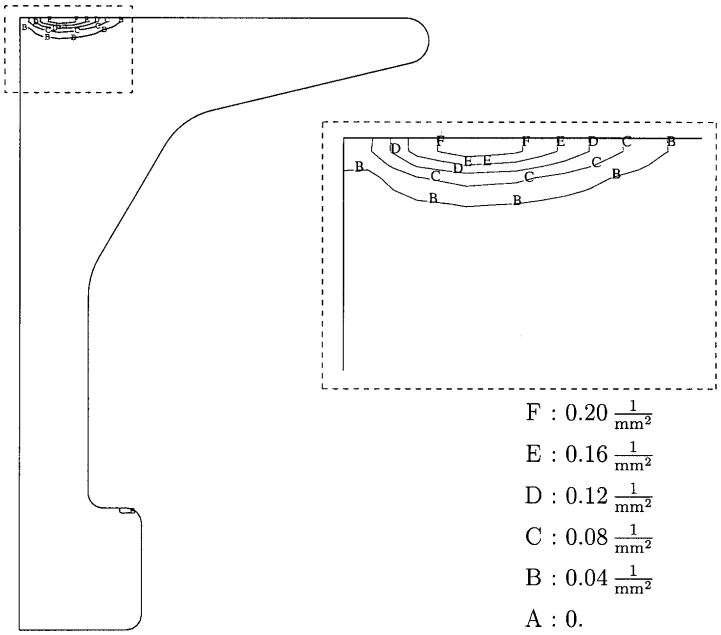


**Figure 5:** Local risk of fracture contours.

This result reflects the general situation that the maximum of the stress field and the maximum of the local risk of fracture do not generally coincide. Additional information is therefore gained from a fracture statistics analysis which turns out to be an indispensable tool for a reliability analysis of ceramic components.

The resulting lifetime distribution for a service life up to $t = 5 \cdot 10^8 \text{s} \approx 16\text{a}$ is shown in Fig. 6 for variations of the heat transfer parameters $h_{hg}$ for the hot gas facing surface and $h_{ca}$ for the cooling air surface, respectively. The sensitivity results shown here are of importance because heat transfer parameters are usually obtained by adapting FE temperature analyses to temperature measurements at selected locations of the component and,

especially for complex geometries, are prone to large uncertainties. Whereas a variation of $h_{ca}$ from 200 to 700 W/(m$^2$K) leads to an increase the failure probability $P_f$ of several orders of magnitude, a variation of $h_{hg}$ between 1100 and 1300 W/(m$^2$K) as shown here has only a minor influence on $P_f$.

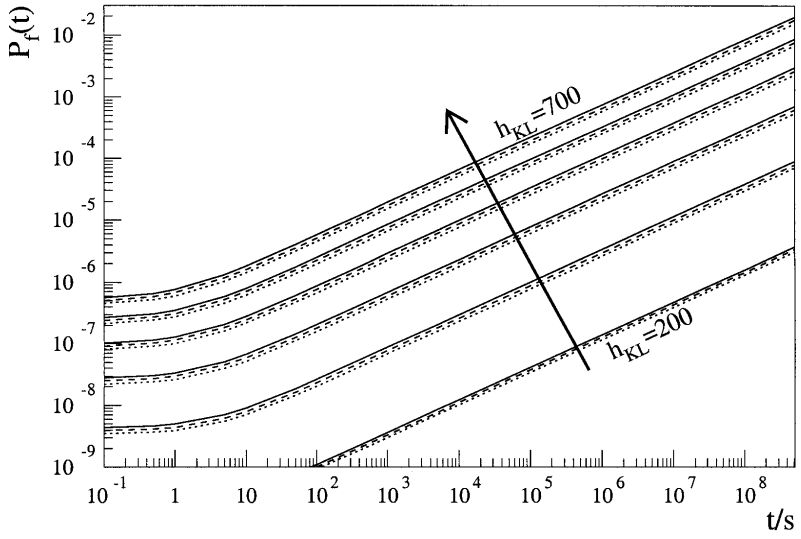


**Figure 6:** Influence of variations in heat transfer conditions on $P_f$.

Apart from stationary normal operating conditions, several transient loading scenarios have to be analysed. One of these is the so-called 'trip', caused by flame extinction and leading to large thermal stresses in the component. A transient analysis of this kind of loading histories was performed using STAU for a typical time scale of about 20 s until maximum stresses are attained. Details of the boundary conditions are given in [12].
For the transient loading analysis, a value of $b$=700 MPa for the Weibull parameter was used. The results are contained in Fig. 7, where the time-dependant value of $P_f$ is shown with and without considering sub-critical crack growth. Even if the thermal stresses are present for quite a short time interval, sub-critical crack growth leads to a failure probability which exceeds that without sub-critical crack growth by a factor of 8.

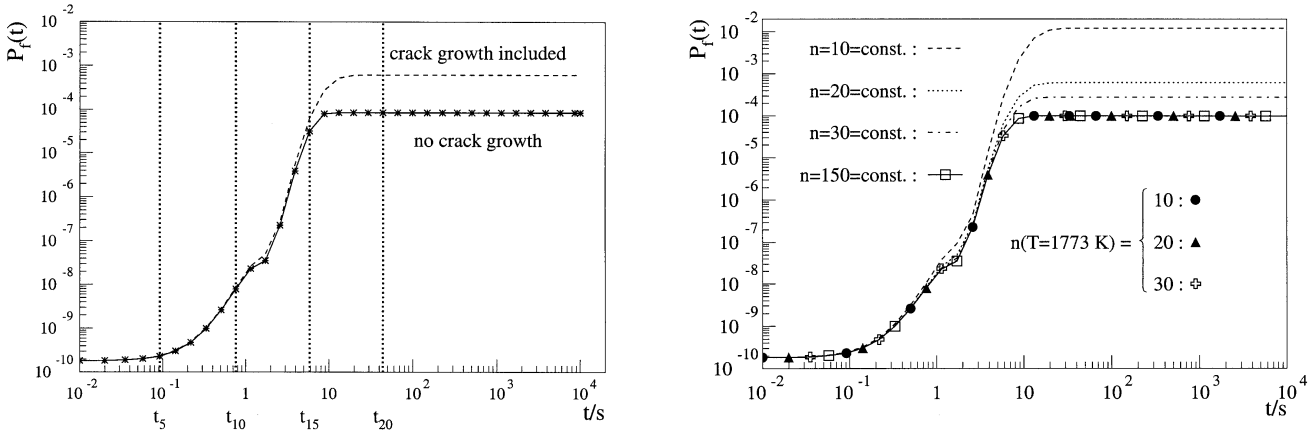


**Figure 7:** Time-dependant failure probability during thermal shock loading.
Left: reference case; right: results for temperature-dependant $n$ in sub-critical crack growth law, Eqn. (7).

The right part of Figure 7 shows results of a parameter study for different values of the exponent $n$ for sub-critical crack growth. The dashed-dotted curves are obtained with $n$-values that are constant over the whole temperature range, whereas the symbols indicate different values for temperatures above T=1773 K. In the present case, variations of $n$ in the high temperature regime do not affect results for the failure probability. For the transient loading case, the local risk of fracture attains its maximum at the outer part of the bolt as shown in Figure 8.

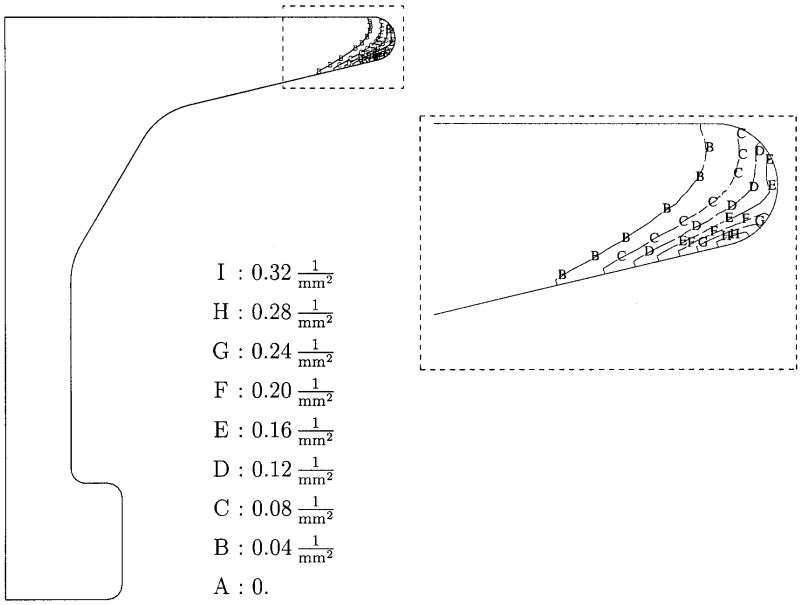


**Figure 8:** Local risk of fracture after end of thermal shock loading caused by a trip scenario.

## SUMMARY

The main features of the STAU postprocessor routine were demonstrated using a high temperature application example. Stationary and transient loading conditions can be assessed by evaluation of local risk of fracture distributions for spontaneous fracture and fracture after sub-critical crack growth. A sensitivity study was performed for those material parameters and boundary conditions for which data are difficult to obtain. Taking the local risk of fracture as a design quantity, critical regions can be identified which will eventually lead to an optimised design.

### *Acknowledgements*

Financial support of the Deutsche Forschungsgemeinschaft, ABB Alstom Power, and Robert Bosch GmbH, is gratefully acknowledged.

### *References*

1. Batdorf, S.B. and Crose, J.G. (1974) *Applied Mechanics* **11**, 459.
2. Batdorf, S.B. and Heinisch, H.L.(1978) *J. Am. Ceram. Soc.* **61**, 355.
3. Evans, A.G. (1978) *J. Am. Ceram. Soc.* **61**, 302.
4. Matsuo, Y. (1981) *JSME* **24**, 290.
5. Brückner-Foit, A., Ziegler, C. (1998). In: *Proc. 22nd Cocoa Beach Conf., American Ceramic Society*, pp. 99-106.
6. Brückner-Foit, A., Heger, A. and Munz, D. (1994). In: *Life Prediction Methods and Data for Ceramic Materials, ASTM STP 1201*, pp. 346-359, Brinkman, C.R. and Duffy, S.F. (Eds.) American Society for Testing and Materials, Philadelphia.
7. Nemeth, N.N., Manderscheid, J. and Gyekenyeshi, J. (1989) NASA TP-2916, Washington D.C.
8. Heiermann, K. et al. (2000) STAU User's Manual, Karlsruhe University, Karlsruhe.
9. Munz, D. and Fett, T. (1999) *Ceramics: mechanical properties, failure behaviour, materials selection*. Springer, Berlin.
10. Brückner-Foit, A., Hülsmeier, P., Riesch-Oppermann, H. and Sckuhr M. (2000). In: *Proc. 45$^{th}$ ASME Gas Turbine and Aeroengine Conference*, (to appear).
11. Brückner-Foit, A., Fett, T., Schirmer, K.-S. and Munz, D. (1996) *J. Europ. Ceram. Soc.* **16**, 1201.
12. Ziegler, C. (1998). *Bewertung der Zuverlässigkeit keramischer Komponenten bei zeitlich veränderlichen Spannungen und bei Hochtemperaturbelastung*, Fortschritt-Berichte VDI Reihe 18 Nr. 238 VDI Verlag Düsseldorf.